Am J Transl Res 2025;17(11):8577-8588
www.ajtr.org /ISSN:1943-8141/AJTR0165035

Original Article

NRF2-mediated autophagic degradation of glycated vimentin in the skin by an elastin-derived peptide

Didier Ritter[1,2], Florian Noguier[2], Roman Bruno[2], Andrea Cavagnino[3], Anais Vaissière[1], Eve Dupas[4], David Piquemal[2], Christophe Desouches[5], Ivan Courtois[6], Armand Azencot[7], Vincent Casoli[8], Pierre Haen[9], Thomas Colson[10], Alain Petit[1], Jean-Daniel Abraham[1]

[1]Regentis-Pharma, 8bis rue Gabriel Voisin, 51100 Reims, France; [2]Acobiom, 1682, rue de la Valsière, CS77394, Cap Delta, 34184 Montpellier, France; [3]OxiProteomics SAS, 2, rue Antoine Etex, 94000 Creteil, France; [4]Kyomed INNOV, 1682, rue de la Valsière, Cap Gamma, 34184 Montpellier, France; [5]Clinique Desouches, 5 Boulevard Notre Dame, 13006 Marseille, France; [6]La maison esthétique, 171 Avenue Victor Hugo, 33110 Le Bouscat, France; [7]Clinique Ferrère, 16 Ter rue Ferrère, 33000 Bordeaux, France; [8]Service de chirurgie plastique, Place Amélie-Raba-Léon, 33000 Bordeaux, France; [9]Hôpital d'instruction des armées Laveran, 34 Bd Laveran, 13013 Marseille, France; [10]122bis cours Gambetta, 13100 Aix en Provence, France

Received April 3, 2025; Accepted October 29, 2025; Epub November 15, 2025; Published November 30, 2025

Abstract: Background: Advanced glycation end products (AGEs) contribute significantly to skin ageing by inducing cross-linking of dermal proteins and promoting oxidative stress. Vimentin, a long-lived intermediate filament protein, is particularly susceptible to glycation and serves as a biomarker for skin ageing and fibrosis. NRF2 (nuclear factor erythroid 2-related factor 2) is a key regulator of cellular defense mechanisms, including antioxidant responses and autophagy. Methods: We evaluated the anti-glycation and pro-regenerative properties of a trifunctional elastin-derived peptide (TFP) in human dermal fibroblasts (*in vitro*), skin explants (*ex vivo*), and in a clinical cosmetic study (*in vivo*). Vimentin glycation and expression were assessed alongside NRF2 pathway activation. Transcriptomic analysis (RNA-seq) in fibroblasts under glyoxal-induced stress identified TFP-regulated genes, further validated by RT-qPCR in skin explants. Results: TFP reduced vimentin glycation across all models. In skin explants, total vimentin levels decreased without changes in *VIM* mRNA expression, suggesting enhanced degradation rather than transcriptional repression. TFP activated the NRF2 pathway, leading to modulation of genes involved in protein homeostasis, including autophagy, proteasomal degradation and anti-inflammatory regulation. Clinical results supported the anti-wrinkle and anti-ageing effects of TFP. Conclusion: TFP activates NRF2-mediated detoxification and protein clearance pathways, facilitating the removal of glycated vimentin. These results highlight TFP's anti-ageing, anti-fibrotic, and anti-inflammatory potential, positioning it as a promising therapeutic candidate for ageing-related skin conditions and disorders associated with proteostasis imbalance.

Keywords: Elastokines, AGEs, CML (carboxymethyllysine), proteostasis, UPR (Unfolded Protein Response), UPS (Ubiquitin Proteasome System)

Introduction

Skin ageing is characterized by hallmark features such as loss of elasticity, the appearance of wrinkles, dryness, and cellular senescence [1]. In recent years, numerous studies have identified advanced glycation end products (AGEs) as key contributors to skin ageing. AGEs are formed through glycoxidation (also referred to as glycation), a complex, slow, non-enzymatic process (known as the Maillard reaction) involving the spontaneous reaction between free amino groups of proteins and reducing sugars such as glucose or ribose. This leads to the formation of an unstable Schiff base, which subsequently rearranges into more stable ketoamines - known as Amadori products. These intermediates undergo further irreversible reactions including oxidation, polymerization, dehydration, and cross-linking, ultimately resulting in AGE formation [2].

In the skin, AGEs generate novel residues or cross-links between dermal matrix molecules, contributing significantly to the loss of tissue elasticity. The most abundant AGEs identified in

https://doi.org/10.62347/ZICX2570

cutaneous tissue include carboxymethyl lysine (CML), carboxyethyl lysine (CEL), and fructoselysine. Receptors for AGEs (RAGEs) are expressed in both the epidermis and dermis, with higher levels observed in sun-exposed regions [3]. In addition to endogenous formation, AGEs derived from smoking and dietary intake may also play a role in skin aging [4-7].

Glycoxidation therefore plays a central role in intrinsic skin ageing by promoting cross-linking within the dermal extracellular matrix, leading to reduced elasticity and altered tissue properties during aging [8]. Glycation modifies the biomechanical and functional characteristics of biological macromolecules - affecting proteins, lipids, and nucleic acids. These modifications can alter protein conformation and solubility, disrupt enzyme-substrate interactions, impair DNA binding and regulation, and affect protein-protein interactions and epigenetic processes, ultimately compromising essential physiological functions [9]. For instance, glycation-induced cross-linking of collagen and elastin increases tissue stiffness and resistance to degradation by matrix metalloproteinases (MMPs) [10]. Moreover, activation of RAGE has been associated with inflammatory and immune responses, upregulation of MMPs, abnormal melanogenesis, dysregulated cell proliferation, and gene expression changes [11-13], all of which may contribute to the ageing phenotype.

Proteins with low turnover rates, such as collagens I and IV, and long-lived proteins like fibronectin and vimentin, are particularly susceptible to glycation in the skin. Notably, vimentin is extensively modified by CML and CEL, as well as by pentosidine and pyrraline, positioning it as a preferential target of the Maillard reaction in human dermal tissue [14]. Accumulation of glycated vimentin has been observed in fibroblasts from aged skin in vivo. These extracellular matrix alterations lead to changes in fibroblast morphology and distribution, as evidenced by vimentin staining [8]. Thus, vimentin and CML serve as valuable biomarkers for assessing the degree of skin ageing [15, 16]. Therapeutically, targeting elevated vimentin expression and its AGE modifications may offer new avenues for mitigating age-related skin damage [17].

In a previous study, our group demonstrated the anti-wrinkle and regenerative potential of a trifunctional peptide (TFP), which stimulates the expression of type I and type III collagen in dermal fibroblasts, both *in vitro* and *ex vivo* in human skin explants [18, 19]. This TFP was engineered by coupling the collagen-mimetic sequence $(Val\text{-}Gly\text{-}Val\text{-}Ala\text{-}Pro\text{-}Gly)_3$ with the tripeptide GIL (Gly-Ile-Leu), designed to inhibit MMP-1. These moieties were linked via a protease-sensitive peptide linker (RVRL; Arg-Val-Arg-Leu), capable of being recognized by enzymes of the plasminogen system.

In the present study, we investigated the anti-glycation properties of TFP in fibroblasts and skin explants, focusing on vimentin glycation. Using RNA sequencing (RNA-seq), we identified gene expression changes related to autophagy following TFP treatment under glyoxal-induced stress. These findings were validated *ex vivo* by RT-qPCR, demonstrating TFP's efficacy in human skin models.

Materials and methods

In vitro evaluation of CML and glycated vimentin in dermal fibroblasts

Sample preparation: The cells were seeded at 10,000 cells per well (96 well plate) at 37°C, 5% CO_2, 10% FBS (fetal bovine serum) culture medium and maintained in optimal growing conditions for 3 days. After 3 days, the glycation was induced with glyoxal at different dosage (0.1 mM, 0.2 mM, 0.4 mM, 0.6 mM and 0.8 mM) for 24 hours. The TFP peptide was then added at 50 µg/ml for an additional 24 hours. The control group (cells incubated with glyoxal at different dosages) did not receive any treatment, except from the renewal of the culture medium.

Labelling and image acquisition: After treatments, the cells were washed, saturated for non-specific sites (PierceTM in PBS [Phosphate Buffered Saline, pH 7.4 solution]) and fixed on the plate and incubated for 1 hour with primary antibody (Rabbit monoclonal anti-Vimentin - Abcam [ab92547] and Mouse monoclonal anti-CML - R&D Systems [MAB3247]) in a PierceTM solution in PBS. After incubation, the cells were washed with PBS and incubated for 1 hour with the secondary antibody coupled to a fluorochrome (Goat anti-mouse AlexaFluor 488 - Invitrogen [A11001] and Goat anti-Rabbit AlexaFluor 647 - Invitrogen [A21244]) and the

nuclei were labelled with DAPI (4',6-diamino-2-phenylindole). After incubation, the cells were washed with PBS and a series of images were acquired with an epifluorescence microscope (ThermoFisher, Evos M5000, 40X objective). The images were collected and analyzed with the software ImageJ (Rasband, NIH).

Image analysis: The quantification on each image was acquired by the integration of the specific fluorescence signal. The vimentin level was quantified by evaluating the occupied surface above a fluorescence intensity threshold, normalized then on the number of cells. The level of CML was quantified by integration of the signal intensity above a threshold, normalized by the surface of the evaluation area and then by the number of cell nuclei. The levels of glycated vimentin were obtained by the ratio between the quantified intensity signal of CML (RFU/cell) over the occupancy of vimentin (surface/cell). Statistical analyses were carried out using t-test for binary comparison (p-value = 0.05).

Ex vivo evaluation of TFP anti-glycation properties in skin explants

Sample preparation: Skin explants were obtained with the informed consent from abdominal surgery of a 32-year-old female Caucasian donor. The explants were kept alive by culturing on metal grids in medium at 37°C in 5% CO_2, humidified air. The culture medium was renewed every 24 hours, or 48 hours after treatment with glyoxal. After reception, the explants were distributed in 3 experimental groups (n = 3 per group). At Day 0, Day 2, Day 4, the active ingredient was topically applied at the concentration of 50 µg/mL. The glycation inducer (glyoxal, 500 µM) was applied at Day 1 and Day 3 in the culture medium. The control group did not receive any treatment except for the medium renewal. At Day 5, 24 hours after the 3rd treatment with the active ingredient, the explants were sampled: half of each explant was embedded in OCT for cryopreservation and stored at -80°C until analyses and the other half of each explant was flash frozen in liquid nitrogen, stored at -80°C until analyses.

Vimentin glycation detection: In situ analysis of vimentin glycation (CML) was performed by epifluorescence microscopy via specific immunofluorescence detection of independent signals (vimentin, CML) as described above. CML levels (R.F.U./surface) were quantified on the co-localized surface of vimentin above threshold.

Vimentin ELISA: Proteins were extracted from explants and the assessment of Vimentin levels was carried out following the manufacture instructions (colorimetric method; ab246526, Abcam). The total protein quantification was carried out by Bradford assay and equal amounts of total proteins were employed per each measurement. Duplicate of measurement per explant were realized, for a total of 6 measures per condition (2 per single explant). The absorbances were interpolated from the Vimentin standard curve.

Identification and validation of TFP-induced gene expression

Cell culture and RNA purification: Fibroblasts were cultured as described above. After 3 days in optimal growing conditions, the culture medium was renewed without or with TFP added at 50 µg/ml for an additional 48 hours. Cells were then harvested and homogenized in 700 µl QIAzol® Lysis Reagent in a 2 ml SafeLock microcentrifuge tube. Cells were disrupted by mechanical shaking using TissueLyzer II apparatus (Qiagen) 2 × 2 min at 20 Hz. Samples were then incubated 5 minutes at room temperature. Then 140 µl chloroform were added to the homogenate. Tubes were shaken vigorously for 15 s and placed back onto the benchtop for another 2-3 min. Lysates were centrifuged at 12,000 g for 15 min at 4°C in a microcentrifuge. Upper aqueous phase (approximately 350 µl) was carefully transferred to a clean 2 ml microcentrifuge. The rest of the procedure was performed following the manufacturer protocol using QIAcube automated workstation (Qiagen). At the end of the procedure, RNA was eluted using 30 µl of H_2O. A 3 µl sample was aliquoted for quality validation and samples were stored at -80°C. RNA sample concentration and purity was measured using a spectrophotometer NanoDrop ND-1000 (Thermo Scientific). RNA integrity was assessed using Agilent 2200 TapeStation RNA ScreenTape (Agilent Technologies) and RINe score (RNA Integrity Number equivalent) was checked (RINe >6).

RNAseq: RNA-Seq library construction was performed using KAPA mRNA Hyperprep kit (KAPA) using 50 ng total RNA following manufacturer procedures. Briefly, following total RNA extrac-

tion, mRNA was isolated using poly(A) selection, and subsequently, cDNA synthesis was performed. The cDNA fragments underwent end repair, A-tailing, and adapter ligation, followed by PCR amplification to generate the final RNA-Seq libraries. Quality control steps ensured the integrity of the libraries before downstream sequencing analysis. Libraries were indexed and adapted with Illumina P5/P7 for 17 PCR cycles, then quantified before pooling using Qubit (Thermo Scientific) and qualified with LabChip GX (Perkin Elmer). Sequencing was performed on the Illumina Novaseq 6000 in paired-ends (2 × 50 M reads).

Human genome version GRCh38.p13 was used as a reference for bioinformatic analysis. RNASeq data were mapped using Ensembl database release 103 (https://www.ensembl.org). All steps of the pipeline are listed below: Cleaning and trimming using FASTP software (https://www.ncbi.nlm.nih.gov/pmc/articles/PMC6129281/); Quality control using FASTQC software: (http://www.bioinformatics.babraham.ac.uk/projects/fastqc/); Mapping on Human genome with STAR software (https://www.ncbi.nlm.nih.gov/pmc/articles/PMC3530905/) with genome of reference: "Homo_sapiens.GRCh38.dna.primary_assembly.fa" and with annotation: "Homo_sapiens.GRCh38.103.chr.gtf" from Ensembl; Counting of reads for genes with STAR software.

RT-qPCR: cDNA synthesis was performed using ReadyScript™ cDNA Synthesis Mix (Sigma-Aldrich) in 20 µl final reaction volume following the manufacturer protocol. For each sample, 550 ng of RNA were used as RNA matrix for the reverse transcriptase enzyme. cDNA synthesis was performed using 96-well plates in a 20 µl final reaction volume using a Bio-Rad C1000 thermocycler according to the following thermal program: 5 minutes at 25°C, 30 minutes at 42°C, 5 minutes at 85°C. Pure cDNA was stored at -20°C until use.

All qPCR reactions were carried out using 384-well plates in 3 technical replicates. qPCR reactions were carried out on the LightCycler 480 System II (Roche) in a 10 µl final reaction volume. The reaction mix consists of 5 µl of LightCycler 480 SYBR Green I Master Mix 2X (Roche Diagnostics), 4 µl of primers (0.7 µM final concentration) and 1 µl of 1:10 diluted cDNA. qPCR cycling program consisted of a polymerase activation step at 95°C for 10 minutes then followed by 45 cycles of qPCR reaction at 95°C for 3 seconds for denaturation, 60°C for 15 seconds for annealing and 72°C for 15 seconds for extension with fluorescence acquisition at the end of the extension step. At the end, a melting curve was made starting at 65°C up to 97°C with continuous fluorescence acquisition to control amplicon specificity. The measured Ct value of each gene was repeated 3 times, and the standard deviation of the replicate was strictly inferior to 0.5 Ct. The NTC (No Template Control) reaction was performed in the same manner but with replacing the cDNA template with PCR grade water (one technical replicate). Raw Ct data were acquired using the 2nd derivative maximum method on the LightCycler 480 System II instrument (Roche). Analysis of relative gene expression using real-time quantitative PCR data and statistical calculations were done by the $2^{-DeltaDeltaCt}$ method, by considering YWHAZ, PPIB and B2M as housekeeping genes [20].

In vivo study - clinical trial

Design of the clinical trial: This study was performed on human skin tissue obtained from surgical residues in full respect of the Declaration of Helsinki and Article L.1243-4 of the French Public Health Code. The clinical trial was registered under the number ANSM 2016-A00381-50 and was developed as a single-blind, multicenter, randomized and controlled trial conducted on 24 women (from 45 to 70 years old) who applied the two products, cosmetic creams (based on a water/oil emulsion) with or without the TFP (100 µg/ml), either on the right or the left side of the face, twice a day for 28 days. After this period, 21 out of 24 underwent a facelift surgery and the skin samples were recovered for molecular analyses [18].

Collection and treatment of skin removal after face lift: The surgical intervention was performed according to the classical technique of the surgeon. The surgical skin waste, removed during the surgery, correspond to excess skin resulting from the laxity of the skin from the peri-auricular area. One piece of cutaneous excess of each side of the face was retrieved and split in 2 fragments for genomic and proteomic analyses:

• Treatment of skin samples for genomic analyses: The skin pieces from each side of the face (1 to 2 mm^2) were immersed in a preservative solution (RNA later) at room temperature for 2 hours, then refrigerated at 4°C for one night. The samples were stored at -20°C until the analysis by RT-qPCR.

• Treatment of skin samples for proteomic analyses: The skin pieces from each side of the face (≥1 cm^2) were immersed in a solution of 4% formalin at room temperature for 24 hours, then transferred in a solution of ethanol 70% and stored at room temperature before paraffin embedding and analysis. The paraffin sections of approximately 4 µm thick, were cut and placed on Superfrost Plus glass slides, let dry overnight at 45°C (± 3°C) in an air oven before microscopy imaging.

Vimentin immunostaining: The labelling of vimentin on paraffin sections was performed with the OPALTM4-color IHC (immunohistochemistry) kit from PerkinElmer® with the antibody anti-Vimentin (Rabbit polyclonal - Abcam, ab45939). The antibody labelled paraffin sections were then incubated with the fluorophore OPAL 690 (2018 Akoya Biosciences). The nuclei were labelled with DAPI. After a complete ICH and fluorescent labelling, the paraffin sections were scanned by the Vectra Polaris (PerkinElmer) with the objective X20. The visualization, analysis, validation, and quantification of images were performed with the software HALO® (Indicalabs). Thresholds were selected to quantify the positive area of each marker and individual data were generated by the software in an Excel file. The normality of data distribution was verified by the Shapiro-Wilk test, at a risk of 5%. The data were analysed with the Student's t-test for a normal distribution and with a Wilcoxon test in the opposite (*p*-value <0.05).

CML immunostaining: Skin biopsy sections of 5 µm of thickness were obtained using a microtome, fixed on microscope slides and deparaffinated. A saturating step of the non-specific sites was carried out with BSA in PBS (Phosphate Buffered Saline, pH 7.4). The slices were incubated with the primary antibody specific for CML (anti-CML MAB3247; R&D systems) in a solution of Tween-20 0.1% in PBS. The excess of antibodies was eliminated with a sequence of washing steps, then the explants were incubated with the secondary antibody coupled to a fluorochrome (Goat anti-mouse AlexaFluor555, A21422, Invitrogen). The nuclei were labelled by using DAPI (4',6-diamidino-2-phenylindole). Finally, the antibodies and DAPI excess were removed with a sequence of washing steps with Tween-20 0.1% in PBS.

A series of images were acquired with an epifluorescence microscope (ThermoFisher, Evos M5000) using strictly the same acquisition time and resolution (40× objective). The images were collected with all fluorescence signal intensity levels, then analyzed using ImageJ software (Rasband, NIH). The quantification was carried out on each image by the integration of the specific fluorescence signal above threshold, then normalized on the surface of evaluation. Three (3) images per experimental lot were analyzed. A mean value and a standard deviation per experimental lot and per condition (placebo vs treated). The levels of CML were then normalized on each "placebo" lot in order to obtain a relative fold change ratio upon treatment with TFP. Statistical analyses were carried out using t-test for binary comparisons (unpaired, one-tailed, alpha = 0.5).

Statistical analyses

All data are represented as the mean of 3 triplicates and validated with %CV below 25%. The normality of the distribution of the data were verified by the Shapiro-Wilk test, at 5% risk. The data are analysed either with the paired Student t-test for a normal distribution or with the non-parametric Wilcoxon test for paired values in the opposite case.

Results

TFP treatment decreases CML detection and vimentin glycation in vitro

Human fibroblasts were incubated with growing concentrations of glyoxal, with or without supplementation with TFP. As shown in **Figure 1A**, CML immunodetection increases as compared to the control (no stress), and is correlated with glyoxal concentration. TFP treatment significantly decreases CML detection at the highest tested glyoxal concentrations (0.8 mM; p< 0.05). Interestingly, as shown in **Figure 1B**, specific glycation of vimentin, evaluated by immuno-colocalization of CML and vimentin, is decreased in fibroblasts stressed with glyoxal 0.6

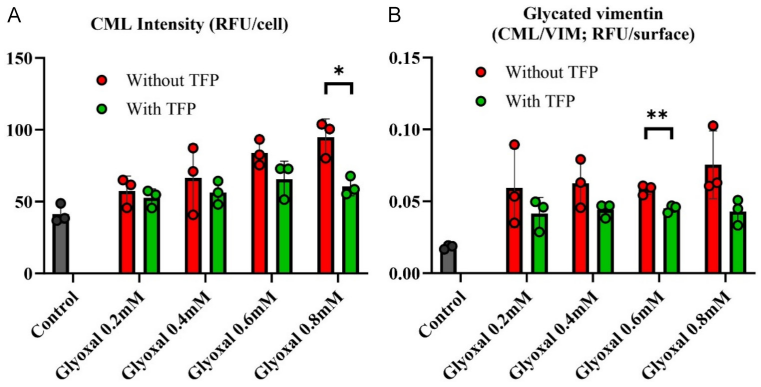

Figure 1. TFP decreases CML formation and vimentin glycation in fibroblasts. After 24 h of treatment with different concentrations of glyoxal, fibroblasts were treated or not with TFP for an additional 24 h. Cells were fixed and labelled with anti-CML antibody (A) and anti-vimentin antibody (B). Green and red bars represent cells respectively grown with or without TFP. N = 3 dot per condition; *: *p*-value <0.05; **: *p*-value <0.01.

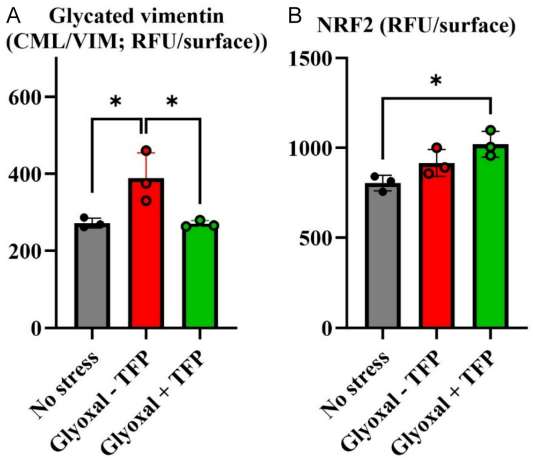

Figure 2. TFP reduces vimentin glycation in skin explants by improving NRF2 nuclear translocation. Skin explants were cultured with or without TFP after glyoxal treatment and labelled with anti-CML and anti-vimentin antibodies (A) or with anti-NRF2 antibody to detect NRF2 nuclear translocation (B). Labelling intensities in triplicates are presented according to skin explants treatment; gray: no stress; red: stress without TFP; n = 3 dot per condition; green: stress with TFP; *: *p*-value <0.05.

mM upon TFP treatment (in green as compared to untreated in red, p<0.01).

TFP decreases vimentin glycation through NRF2 pathway activation

Skin explants were cultured *ex vivo* in different media by inducing glycation or not with glyoxal, with or without TFP treatment. Vimentin glycation and NRF2 nuclear localization were evaluated by coimmunolabelling. As shown in **Figure 2A** (and Supplementary Figure 1), vimentin glycation is increased in glyoxal-treated explants (p<0.05) and decreased upon TFP treatment (p<0.05), confirming the results obtained in fibroblasts. Using the same skin explants, NRF2 nuclear localization was evaluated by specific immunodetection. As shown in **Figure 2B** (and in Supplementary Figure 2), NRF2 nuclear translocation is significantly increased in TFP-treated glyoxal-stressed explants as compared to the untreated condition (p<0.05).

TFP modulates the expression of genes involved in UPR

A comparative transcriptome analysis based on TFP- or placebo-treated fibroblasts led to the identification of 546 significant genes involved in the regulation of oxidative stress, inflammation and autophagy (Supplementary Figure 3). After pathway analysis focusing on protein homeostasis, 45 genes were tested by RT-qPCR for technical validation (reproducibility, repeatability, sensitivity). Importantly, each primer was designed according to previous RNAseq results (Supplementary Figure 4). Thirteen (13) genes were validated in untreated fibroblasts and skin extracts and further tested in glyoxal-treated skin explants. As shown in **Figure 3**, glyoxal induced upregulation of CXCL1 (p<0.01) and DNAJC10 (p<0.05) expression, and downregulation of DNAJB14 (p<0.05), UBE2D3 (p<0.05), PSMD12 (p<0.05) and RNF19A (p<0.001) expression. TFP was allowed to counteract glyoxal effects, by downregulating CXCL1 (p<0.0001) and DNAJC10 (p<0.01) expression, while upregulating DNAJB14 (p<0.01), UBE3A (p<0.05), UBE2D3 (p<0.05), DRAM2 (p<0.05), PSMD12 (p<0.05), TRIM23 (p<0.05) and RNF19A (p<0.05). Noteworthy, by analyzing extracted RNA from the same samples, no difference in VIM expression was observed.

TFP decreases vimentin glycation in vivo

Female volunteers (n = 24) were included in a 28 days cosmetic clinical trial followed by surgi-

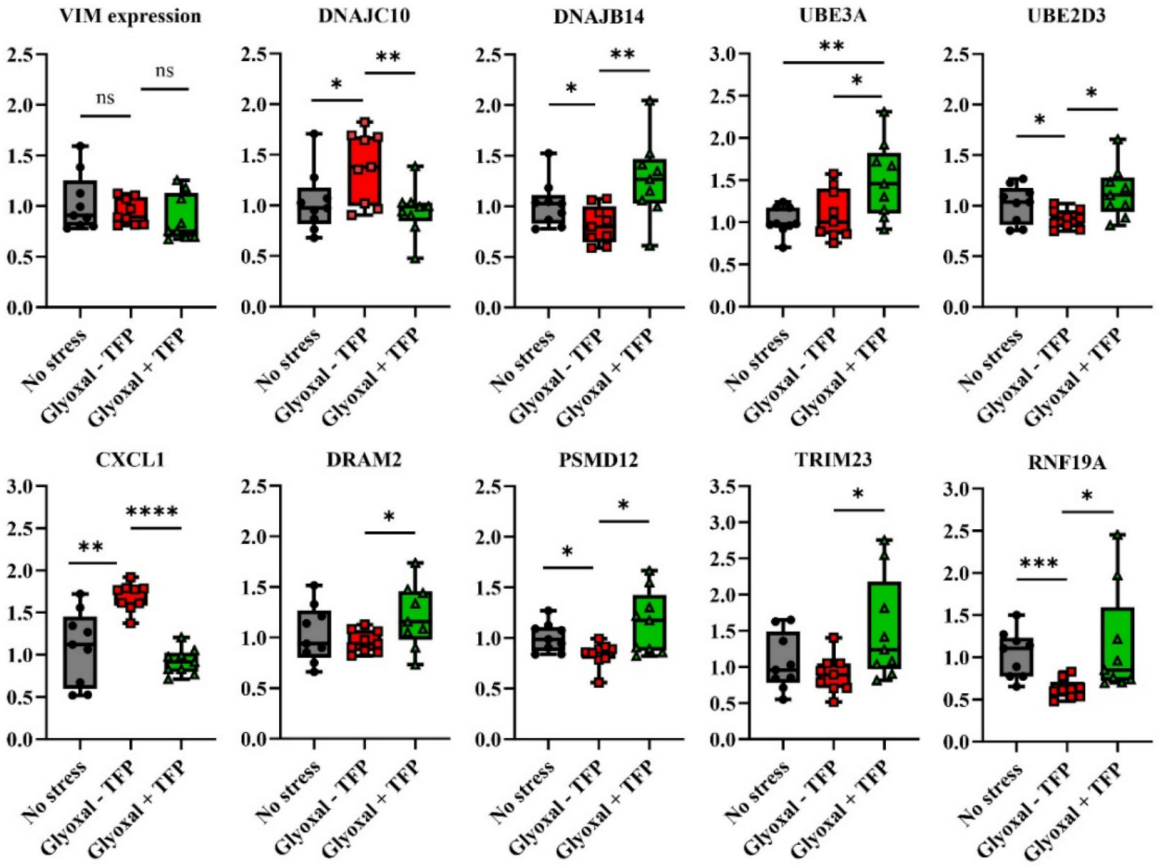

Figure 3. TFP counteracts glyoxal-induced gene transcription in skin explants. RNAseq-based specific primers were designed to perform RT-qPCR in skin explants cultured with (green box) or without (red box) TFP after glyoxal treatment; n = 3 wells per culture condition; n = 3 technical replicates; *: *p*-value <0.05; **: *p*-value <0.01; ***: *p*-value <0.001; ****: *p*-value <0.0001.

cal lifting as previously described [18]. As shown in Supplementary Figure 5, three of them were discarded from the study due to absence of surgical lifting. After sample treatment, four of them did not fulfill quality for the requirements for rigorous immunostaining analysis (2 due to a lack of triplicated data, 2 due to a lack of reproducibility of the triplicates). The 17 remaining volunteers were analyzed for vimentin (**Figure 4A** and Supplementary Figure 6) and CML (**Figure 4B** and Supplementary Figure 7) expression, showing a significant decrease of vimentin glycation ($p<0.05$) in human samples upon TFP treatment, as compared to placebo treatment.

Discussion

To our knowledge, this is the first study to demonstrate the modulation of glycated vimentin degradation by an elastin-derived peptide through NRF2 pathway activation. We showed that TFP significantly reduced vimentin glycation *in vitro* (fibroblast model), *ex vivo* (human skin explants), and *in vivo* in a cosmetic study involving patients who underwent surgical lifting after 28 days of topical treatment. Notably, in skin explants, TFP treatment led to a decrease in total vimentin levels without altering *VIM* gene expression, while promoting NRF2 nuclear translocation. These results suggest that the reduction in vimentin levels is primarily driven by enhanced degradation mechanisms via NRF2 activation. RNA sequencing in fibroblasts exposed to glyoxal stress, followed by validation via RT-qPCR in skin explants, revealed a panel of NRF2-regulated genes modulated by TFP treatment.

We acknowledge certain limitations of our study, particularly the small sample size in each experimental model. Each *in vitro* and *ex vivo*

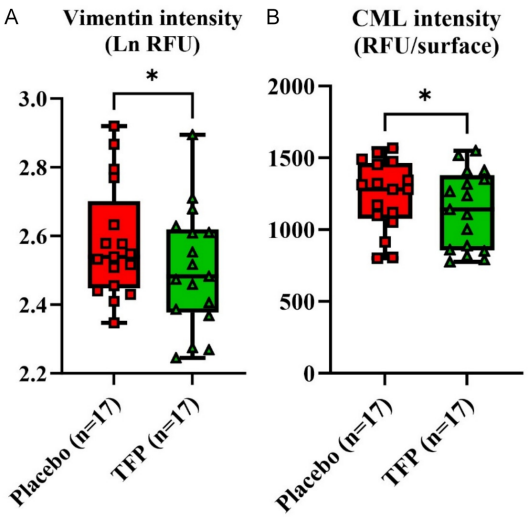

Figure 4. TFP decreases glycated vimentin in vivo. Skin biopsies from face lifting of the 17 volunteers were analyzed by immunolabelling using specific anti-vimentin antibody (A) or specific anti-CML antibody (B); results are presented as box-plot representation of the labelling intensity in paired samples from the 17 patients; red: labelling intensity in the 17 extracts from placebo-treated hemi-faces; green: labelling intensity in the 17 extracts from TFP-treated hemi-faces; *: *p*-value <0.05.

assay was performed in triplicate without replication, and the clinical trial included a limited cohort of 17 volunteers post-selection.

Strict technical standards were applied to ensure the reproducibility and reliability of results, with a coefficient of variation (CV) maintained below 25%. Furthermore, the design of the clinical trial - using a hemi-face application for each subject - enabled robust within-subject comparisons using paired *t*-tests. Most importantly, *in vitro*, *ex vivo*, and *in vivo* results all converged toward a consistent conclusion: TFP modulates the NRF2 pathway and facilitates the degradation of glycated vimentin.

The NRF2 signaling pathway plays a pivotal role in cellular redox homeostasis and is one of the primary defense mechanisms against glycoxidative stress. Upon activation, NRF2 translocates to the nucleus, where it binds to antioxidant response elements (AREs) in the promoters of target genes [21]. High levels of NRF2 are expressed in skin cells including keratinocytes and melanocytes [22]. Genes activated by NRF2 are involved in a range of cellular processes, including protein quality control, trafficking, macro-autophagy, and disulfide bond regulation [23].

One key gene identified in our study is *DNAJC-10*, a member of the protein disulfide isomerase (PDI) family. It plays a role in disulfide bond reduction and rearrangement [24]. *DNAJC10*-deficient hepatocytes have been shown to produce large amounts of reactive oxygen species (ROS) [25]. We observed that glyoxal stress increased *DNAJC10* expression as part of an antioxidant response, likely through upregulated reductase activity. TFP treatment restored *DNAJC10* to basal levels, suggesting compensatory activation of alternative protective pathways.

Beyond antioxidant responses, NRF2 is implicated in protein homeostasis, particularly through autophagy and the unfolded protein response (UPR) [26]. Several genes downregulated by glyoxal and subsequently restored by TFP are involved in proteostasis:

- TRIM23, a member of the TRIM family of E3 ubiquitin ligases, is essential for autophagy-mediated viral restriction [27, 28].

- DRAM2 regulates p53-mediated cell death [29] and autophagy [30].

- DNAJB14 facilitates degradation of misfolded membrane proteins via the ubiquitin-proteasome system (UPS) [31], and plays a role in ER protein reflux during UPR [32]. In Huntington's disease models, *DNAJB14* improves proteostasis by increasing aggregate mobility [33].

- UBE2D3, an E2 ubiquitin-conjugating enzyme, regulates autophagic flux and protein quality control [34, 35].

- UBE3A promotes degradation of misfolded proteins and is recruited to aggresomes. It can interact directly with vimentin and FRMD3 to trigger its polyubiquitin-mediated degradation [36, 37].

- PSMD12, a subunit of the 26S proteasome complex, contributes to protein turnover, cell cycle control, and DNA repair [38, 39].

Additionally, RNF19A is involved in proteasomal degradation through K48-linked ubiquitination. Its expression is associated with regulation of inflammation via degradation of TRAF6, a key

activator of NF-κB and MAPK pathways cells [40, 41]. TFP-induced upregulation of *RNF19A* may therefore contribute to its anti-inflammatory effects. NRF2 is increasingly recognized as a modulator of cytokine production [42]. Supporting our findings, a recent transcriptomic study in human retinal endothelial cells exposed to AGEs identified CXCL1 - a neutrophil chemoattractant - as one of the top upregulated genes [43], in line with the inflammatory response observed in our glyoxal model.

Interestingly, elastin-derived peptides such as VGVAPG have previously been shown to activate autophagy via PPARγ in neuroblastoma cells [44], supporting the hypothesis that TFP - also elastin-derived - may similarly enhance autophagy and/or aggrephagy to facilitate the clearance of glycated proteins such as vimentin.

The vimentin filament network is integral to cellular architecture, signal transduction, and the epithelial-mesenchymal transition (EMT) [45, 46]. Vimentin participates in aggresome formation, surrounding ubiquitinated protein aggregates with a filamentous cage structure [47, 48]. Glycation of vimentin induces its perinuclear aggregation and disrupts fibroblast contractility [16, 17, 49]. Retinoic acid, a well-known anti-ageing compound, also decreases vimentin levels in skin explants [15]. Vimentin has been proposed as a therapeutic target in age-related diseases and is associated with fibrotic profiles. Elevated vimentin levels have been observed in renal fibrosis [50], while negative pressure wound therapy leads to its reduction in skin tissue [51]. Thus, treatments that reduce vimentin levels may possess both anti-ageing and anti-fibrotic potential.

Through activation of the NRF2 pathway, TFP may also regulate aggresome formation, contributing to skin homeostasis and cellular differentiation under both normal and pathological conditions [21, 52, 53]. For example, psoriasis is associated with elevated glycoxidative stress [54], and atopic dermatitis shows impaired NRF2 activation in affected epidermal regions [55]. NRF2 activators have also shown promise in chronic wound healing, restoring redox homeostasis and promoting tissue regeneration [56].

The involvement of AGEs in diabetic complications is well documented. In particular, AGE-induced endothelial-to-mesenchymal transition (EndMT) contributes to fibrosis in diabetic tissues, including the pancreatic islets [57]. Oxidative stress plays a central role in the development of diabetic foot ulcers (DFUs), and NRF2 activation has emerged as a promising therapeutic strategy to restore redox balance and improve healing outcomes [58].

In conclusion, TFP counteracts AGE-induced gene expression changes by activating NRF2 and promoting macroautophagy. This results in reduced levels of glycated vimentin and improved cellular homeostasis. Our findings highlight TFP's anti-ageing, anti-fibrotic, and anti-inflammatory properties, supporting its potential application in a broad range of dermatological conditions, including psoriasis, atopic dermatitis, and impaired wound healing.

Disclosure of conflict of interest

AP and AV are Regentis Pharma employees; DR and JDA are consulting experts for Regentis Pharma. FN, RB, DR and DP are Acobiom employees; ED is a Kyomed employee; AC is an Oxiproteomics employee.

Address correspondence to: Jean-Daniel Abraham, Regentis-Pharma, 8bis rue Gabriel Voisin, 51100 Reims, France. E-mail: jean-daniel.abraham@regentis-pharma.com

References

[1] Zhang S and Duan E. Fighting against skin aging: the way from bench to bedside. Cell Transplant 2018; 27: 729-738.

[2] Gkogkolou P and Böhm M. Advanced glycation end products: key players in skin aging? Dermatoendocrinol 2012; 4: 259-270.

[3] Lohwasser C, Neureiter D, Weigle B, Kirchner T and Schuppan D. The receptor for advanced glycation end products is highly expressed in the skin and upregulated by advanced glycation end products and tumor necrosis factor-alpha. J Invest Dermatol 2006; 126: 291-299.

[4] Goldberg T, Cai W, Peppa M, Dardaine V, Baliga BS, Uribarri J and Vlassara H. Advanced glycoxidation end products in commonly consumed foods. J Am Diet Assoc 2004; 104: 1287-1291.

[5] Mizutari K, Ono T, Ikeda K, Kayashima K and Horiuchi S. Photo-enhanced modification of human skin elastin in actinic elastosis by N(epsilon)-(carboxymethyl)lysine, one of the glycoxidation products of the Maillard reaction. J Invest Dermatol 1997; 108: 797-802.

[6] Nicholl ID, Stitt AW, Moore JE, Ritchie AJ, Archer DB and Bucala R. Increased levels of advanced glycation endproducts in the lenses and blood vessels of cigarette smokers. Mol Med 1998; 4: 594-601.
[7] Uribarri J, Cai W, Peppa M, Goodman S, Ferrucci L, Striker G and Vlassara H. Circulating glycotoxins and dietary advanced glycation endproducts: two links to inflammatory response, oxidative stress, and aging. J Gerontol A Biol Sci Med Sci 2007; 62: 427-433.
[8] Pageon H and Asselineau D. An in vitro approach to the chronological aging of skin by glycation of the collagen: the biological effect of glycation on the reconstructed skin model. Ann N Y Acad Sci 2005; 1043: 529-532.
[9] Baynes JW. The Maillard hypothesis on aging: time to focus on DNA. Ann N Y Acad Sci 2002; 959: 360-367.
[10] Paul RG and Bailey AJ. Glycation of collagen: the basis of its central role in the late complications of ageing and diabetes. Int J Biochem Cell Biol 1996; 28: 1297-1310.
[11] DeGroot J. The AGE of the matrix: chemistry, consequence and cure. Curr Opin Pharmacol 2004; 4: 301-305.
[12] Lee EJ, Kim JY and Oh SH. Advanced glycation end products (AGEs) promote melanogenesis through receptor for AGEs. Sci Rep 2016; 6: 27848.
[13] Zhu P, Ren M, Yang C, Hu YX, Ran JM and Yan L. Involvement of RAGE, MAPK and NF-κB pathways in AGEs-induced MMP-9 activation in HaCaT keratinocytes. Exp Dermatol 2012; 21: 123-129.
[14] Kueper T, Grune T, Muhr GM, Lenz H, Wittern KP, Wenck H, Stäb F and Blatt T. Modification of vimentin: a general mechanism of nonenzymatic glycation in human skin. Ann N Y Acad Sci 2008; 1126: 328-332.
[15] Kim SH, Kim JH, Suk JM, Lee YI, Kim J, Lee JH and Lee KH. Identification of skin aging biomarkers correlated with the biomechanical properties. Skin Res Technol 2021; 27: 940-947.
[16] Kueper T, Grune T, Prahl S, Lenz H, Welge V, Biernoth T, Vogt Y, Muhr GM, Gaemlich A, Jung T, Boemke G, Elsässer HP, Wittern KP, Wenck H, Stäb F and Blatt T. Vimentin is the specific target in skin glycation. Structural prerequisites, functional consequences, and role in skin aging. J Biol Chem 2007; 282: 23427-23436.
[17] Shin JU, Lee WJ, Oh SH, Kim DY, Kim DS, Jung I and Lee JH. Altered vimentin protein expression in human dermal microvascular endothelial cells after ultraviolet or intense pulsed light treatment. Lasers Surg Med 2014; 46: 431-438.
[18] Abraham JD, Vaissière A, Desouches C, Thiery G, Bertrand B, Alfandari B, Courtois I, Azencot A, Casoli V, Haen P, Colson T, Hornebeck W and Ritter D. Clinical validation of an elastin-derived trifunctional peptide for skin regeneration. Am J Transl Res 2023; 15: 4620-4628.
[19] Attia-Vigneau J, Terryn C, Lorimier S, Sandre J, Antonicelli F and Hornebeck W. Regeneration of human dermis by a multi-headed peptide. J Invest Dermatol 2014; 134: 58-67.
[20] Livak KJ and Schmittgen TD. Analysis of relative gene expression data using real-time quantitative PCR and the 2(-Delta Delta C(T)) method. Methods 2001; 25: 402-408.
[21] Motohashi H and Yamamoto M. Nrf2-Keap1 defines a physiologically important stress response mechanism. Trends Mol Med 2004; 10: 549-557.
[22] Panieri E, Telkoparan-Akillilar P and Saso L. NRF2, a crucial modulator of skin cells protection against vitiligo, psoriasis, and cancer. Biofactors 2023; 49: 228-250.
[23] Liu P, Kerins MJ, Tian W, Neupane D, Zhang DD and Ooi A. Differential and overlapping targets of the transcriptional regulators NRF1, NRF2, and NRF3 in human cells. J Biol Chem 2019; 294: 18131-18149.
[24] Robinson PJ, Pringle MA, Fleming B and Bulleid NJ. Distinct role of ERp57 and ERdj5 as a disulfide isomerase and reductase during ER protein folding. J Cell Sci 2023; 136: jcs260656.
[25] Hong DG, Song GY, Eom CB, Ahn JH, Kim SM, Shim A, Han YH, Roh YS, Han CY, Bae EJ, Ko HJ and Yang YM. Loss of ERdj5 exacerbates oxidative stress in mice with alcoholic liver disease via suppressing Nrf2. Free Radic Biol Med 2022; 184: 42-52.
[26] Tonelli C, Chio IIC and Tuveson DA. Transcriptional regulation by Nrf2. Antioxid Redox Signal 2018; 29: 1727-1745.
[27] Sparrer KMJ, Gableske S, Zurenski MA, Parker ZM, Full F, Baumgart GJ, Kato J, Pacheco-Rodriguez G, Liang C, Pornillos O, Moss J, Vaughan M and Gack MU. TRIM23 mediates virus-induced autophagy via activation of TBK1. Nat Microbiol 2017; 2: 1543-1557.
[28] Xiao M, Li J, Liu Q, He X, Yang Z and Wang D. Expression and role of TRIM2 in human diseases. Biomed Res Int 2022; 2022: 9430509.
[29] Yoon JH, Her S, Kim M, Jang IS and Park J. The expression of damage-regulated autophagy modulator 2 (DRAM2) contributes to autophagy induction. Mol Biol Rep 2012; 39: 1087-1093.
[30] Yang KE, Nam SB, Jang M, Park J, Lee GE, Cho YY, Jang BC, Lee CJ and Choi JS. Ginsenoside Rb2 suppresses cellular senescence of human dermal fibroblasts by inducing autophagy. J Ginseng Res 2023; 47: 337-346.

[31] Sopha P, Kadokura H, Yamamoto Y, Takeuchi M, Saito M, Tsuru A and Kohno K. A novel mammalian ER-located J-protein, DNAJB14, can accelerate ERAD of misfolded membrane proteins. Cell Struct Funct 2012; 37: 177-187.
[32] da Purificação AD, Debbas V, Tanaka LY, de Mello Gabriel GV, Júnior JW, De Bessa TC, Garcia-Rosa S, Laurindo FRM and Oliveira PVS. DNAJB12 and DNJB14 are non-redundant Hsp40 redox chaperones involved in endoplasmic reticulum protein reflux. Biochim Biophys Acta Gen Subj 2024; 1868: 130502.
[33] Rozales K, Younis A, Saida N, Meller A, Goldman H, Kellerman L, Heinrich R, Berlin S and Shalgi R. Differential roles for DNAJ isoforms in HTT-polyQ and FUS aggregation modulation revealed by chaperone screens. Nat Commun 2022; 13: 516.
[34] Yalçin Z, Koot D, Bezstarosti K, Salas-Lloret D, Bleijerveld OB, Boersma V, Falcone M, González-Prieto R, Altelaar M, Demmers JAA and Jacobs JJL. Ubiquitinome profiling reveals in vivo UBE2D3 targets and implicates UBE2D3 in protein quality control. Mol Cell Proteomics 2023; 22: 100548.
[35] Wang X, Yang P, Jiang Y, Xu Y, Wang N, Rao P, Yang L, Sun L and Lu D. UBE2D3 contributes to myocardial ischemia-reperfusion injury by regulating autophagy in dependence of p62/SQSTM1. Cell Signal 2021; 87: 110118.
[36] Shao W, Li J, Piao Q, Yao X, Li M, Wang S, Song Z, Sun Y, Zheng L, Wang G, Liu L, Yu C, Huang Y, Bao Y and Sun L. FRMD3 inhibits the growth and metastasis of breast cancer through the ubiquitination-mediated degradation of vimentin and subsequent impairment of focal adhesion. Cell Death Dis 2023; 14: 13.
[37] Mishra A, Godavarthi SK, Maheshwari M, Goswami A and Jana NR. The ubiquitin ligase E6-AP is induced and recruited to aggresomes in response to proteasome inhibition and may be involved in the ubiquitination of Hsp70-bound misfolded proteins. J Biol Chem 2009; 284: 10537-10545.
[38] Küry S, Besnard T, Ebstein F, Khan TN, Gambin T, Douglas J, Bacino CA, Craigen WJ, Sanders SJ, Lehmann A, Latypova X, Khan K, Pacault M, Sacharow S, Glaser K, Bieth E, Perrin-Sabourin L, Jacquemont ML, Cho MT, Roeder E, Denommé-Pichon AS, Monaghan KG, Yuan B, Xia F, Simon S, Bonneau D, Parent P, Gilbert-Dussardier B, Odent S, Toutain A, Pasquier L, Barbouth D, Shaw CA, Patel A, Smith JL, Bi W, Schmitt S, Deb W, Nizon M, Mercier S, Vincent M, Rooryck C, Malan V, Briceño I, Gómez A, Nugent KM, Gibson JB, Cogné B, Lupski JR, Stessman HAF, Eichler EE, Retterer K, Yang Y, Redon R, Katsanis N, Rosenfeld JA, Kloetzel PM, Golzio C, Bézieau S, Stankiewicz P and Isidor B. De novo disruption of the proteasome regulatory subunit PSMD12 causes a syndromic neurodevelopmental disorder. Am J Hum Genet 2017; 100: 689.
[39] Wang Z, Li Z, Xu H, Liao Y, Sun C, Chen Y, Sheng M, Lan Q and Wang Z. PSMD12 promotes glioma progression by upregulating the expression of Nrf2. Ann Transl Med 2021; 9: 700.
[40] Wu C, Su Z, Lin M, Ou J, Zhao W, Cui J and Wang RF. NLRP11 attenuates Toll-like receptor signalling by targeting TRAF6 for degradation via the ubiquitin ligase RNF19A. Nat Commun 2017; 8: 1977.
[41] Niwa J, Ishigaki S, Doyu M, Suzuki T, Tanaka K and Sobue G. A novel centrosomal ring-finger protein, dorfin, mediates ubiquitin ligase activity. Biochem Biophys Res Commun 2001; 281: 706-713.
[42] Kobayashi EH, Suzuki T, Funayama R, Nagashima T, Hayashi M, Sekine H, Tanaka N, Moriguchi T, Motohashi H, Nakayama K and Yamamoto M. Nrf2 suppresses macrophage inflammatory response by blocking proinflammatory cytokine transcription. Nat Commun 2016; 7: 11624.
[43] Monickaraj F, Acosta G, Cabrera AP and Das A. Transcriptomic profiling reveals chemokine CXCL1 as a mediator for neutrophil recruitment associated with blood-retinal barrier alteration in diabetic retinopathy. Diabetes 2023; 72: 781-794.
[44] Szychowski KA and Skóra B. The elastin-derived peptide (VGVAPG) activates autophagy in neuroblastoma (SH-SY5Y) cells via peroxisome proliferator-activated receptor gamma (PPARγ). Mol Cell Neurosci 2023; 127: 103902.
[45] Vu T and Datta PK. Regulation of EMT in colorectal cancer: a culprit in metastasis. Cancers (Basel) 2017; 9: 171.
[46] Usman S, Waseem NH, Nguyen TKN, Mohsin S, Jamal A, Teh MT and Waseem A. Vimentin is at the heart of Epithelial Mesenchymal Transition (EMT) mediated metastasis. Cancers (Basel) 2021; 13: 4985.
[47] Usman S, Jamal A, Bushaala A, Waseem NH, Al-Dehlawi H, Yeudall WA, Teh MT, Tummala H and Waseem A. Transcriptome analysis reveals vimentin-induced disruption of cell-cell associations augments breast cancer cell migration. Cells 2022; 11: 4035.
[48] Pérez-Sala D, Oeste CL, Martínez AE, Carrasco MJ, Garzón B and Cañada FJ. Vimentin filament organization and stress sensing depend on its single cysteine residue and zinc binding. Nat Commun 2015; 6: 7287.
[49] Sliogeryte K and Gavara N. Vimentin plays a crucial role in fibroblast ageing by regulating biophysical properties and cell migration. Cells 2019; 8: 1164.

[50] Lin Y, Cai F, Wang X, Yang Y, Ren Y, Yao C, Yin X, Zhuang H and Hua Z. FADD phosphorylation contributes to development of renal fibrosis by accelerating epithelial-mesenchymal transition. Cell Cycle 2023; 22: 580-595.
[51] Wu M, Matar DY, Yu Z, Chen Z, Knoedler S, Ng B, Darwish OA, Sohrabi S, Friedman L, Haug V, Murphy GF, Rinkevich Y, Orgill DP and Panayi AC. Continuous NPWT regulates fibrosis in murine diabetic wound healing. Pharmaceutics 2022; 14: 2125.
[52] Pajares M, Cuadrado A and Rojo AI. Modulation of proteostasis by transcription factor NRF2 and impact in neurodegenerative diseases. Redox Biol 2017; 11: 543-553.
[53] Qin S, Jiang C and Gao J. Transcriptional factor Nrf2 is essential for aggresome formation during proteasome inhibition. Biomed Rep 2019; 11: 241-252.
[54] Damasiewicz-Bodzek A and Nowak A. Concentrations of N6-Carboxymethyllysine (CML), N6-Carboxyethyllysine (CEL), and Soluble Receptor for Advanced Glycation End-Products (sRAGE) are increased in psoriatic patients. Biomolecules 2022; 12: 1870.
[55] Koch M, Kockmann T, Rodriguez E, Wehkamp U, Hiebert P, Ben-Yehuda Greenwald M, Stölzl D, Beer HD, Tschachler E, Weidinger S, Werner S and Auf dem Keller U. Quantitative proteomics identifies reduced NRF2 activity and mitochondrial dysfunction in atopic dermatitis. J Invest Dermatol 2023; 143: 220-231, e7.
[56] Victor P, Sarada D and Ramkumar KM. Pharmacological activation of Nrf2 promotes wound healing. Eur J Pharmacol 2020; 886: 173395.
[57] Tsai PS, Chiu CY, Sheu ML, Yang CY, Lan KC and Liu SH. Advanced glycation end products activated endothelial-to-mesenchymal transition in pancreatic islet endothelial cells and triggered islet fibrosis in diabetic mice. Chem Biol Interact 2021; 345: 109562.
[58] Song J, Liu A, Liu B, Huang W, Jiang Z, Bai X, Hu L, Zheng S, Guo S, Wu J and Chen Q. Natural biologics accelerate healing of diabetic foot ulcers by regulating oxidative stress. Front Biosci (Landmark Ed) 2022; 27: 285.

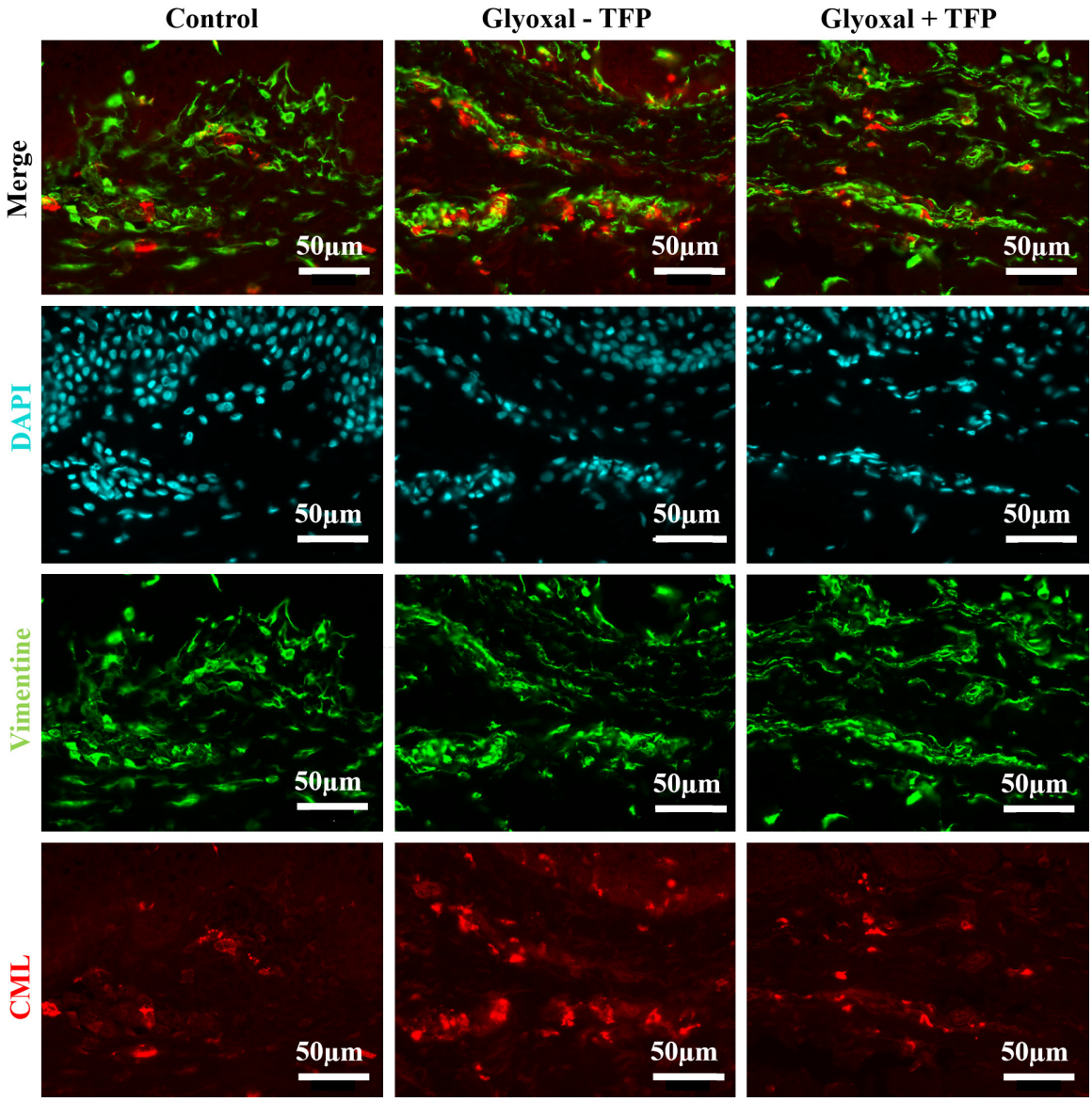

Supplementary Figure 1. TFP reduces vimentin glycation in skin explants. Skin explants were cultured with or without TFP after glyoxal treatment and labelled with anti-CML and anti-vimentin antibodies; The CML signal (in red), the Vimentin signal (in green) and their superposition (in yellow) are presented. The nuclear labelling (DAPI, in cyan) is presented as superposed signal.

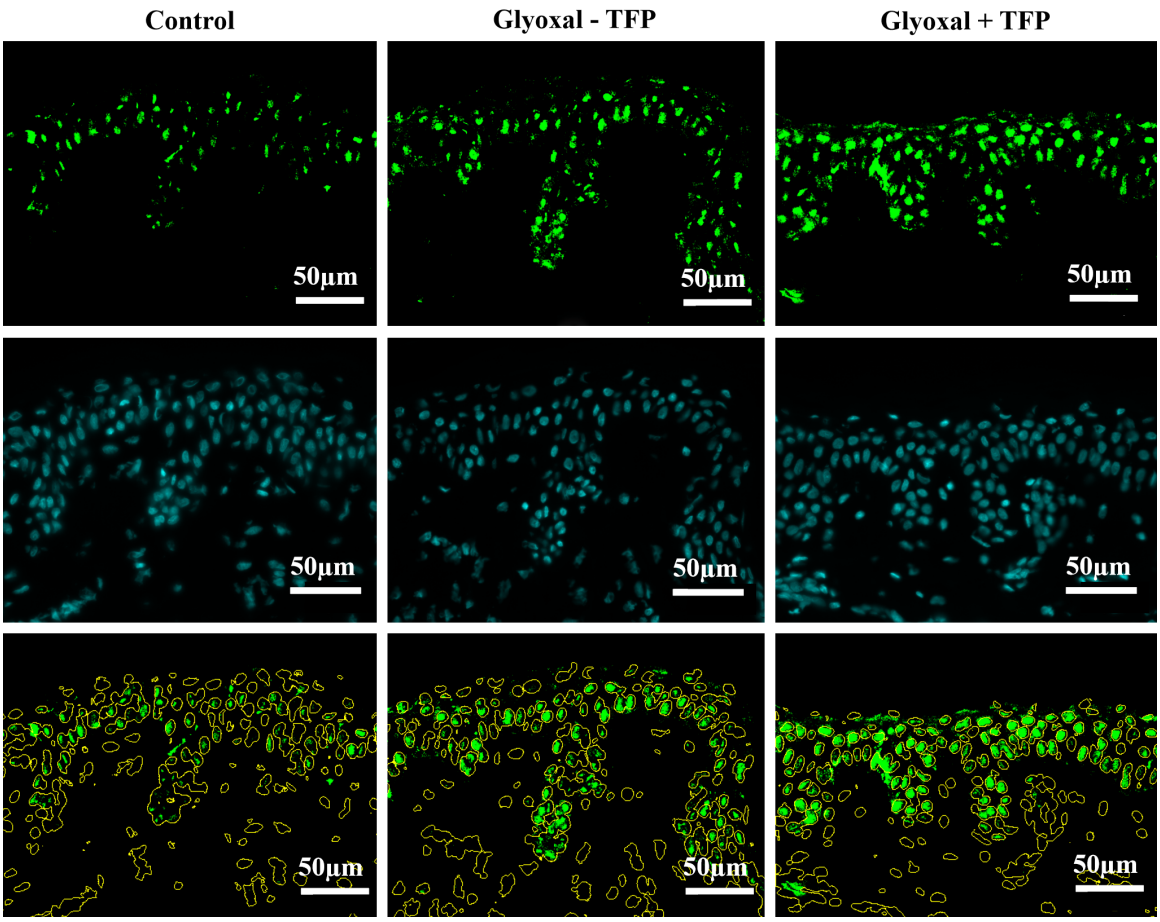

Supplementary Figure 2. TFP improves NRF2 nuclear translocation in skin explants. Skin explants were cultured with or without TFP after glyoxal treatment and were labelled with anti-NRF2 antibody to detect NRF2 nuclear translocation. The fluorescence emission signal for NRF2 on nuclear region (automatic detection) is presented in green. Nuclear detection is presented in cyan (DAPI). The nuclear regions are evidenced by yellow dotted lines and superposed to the NRF2 signal over threshold.

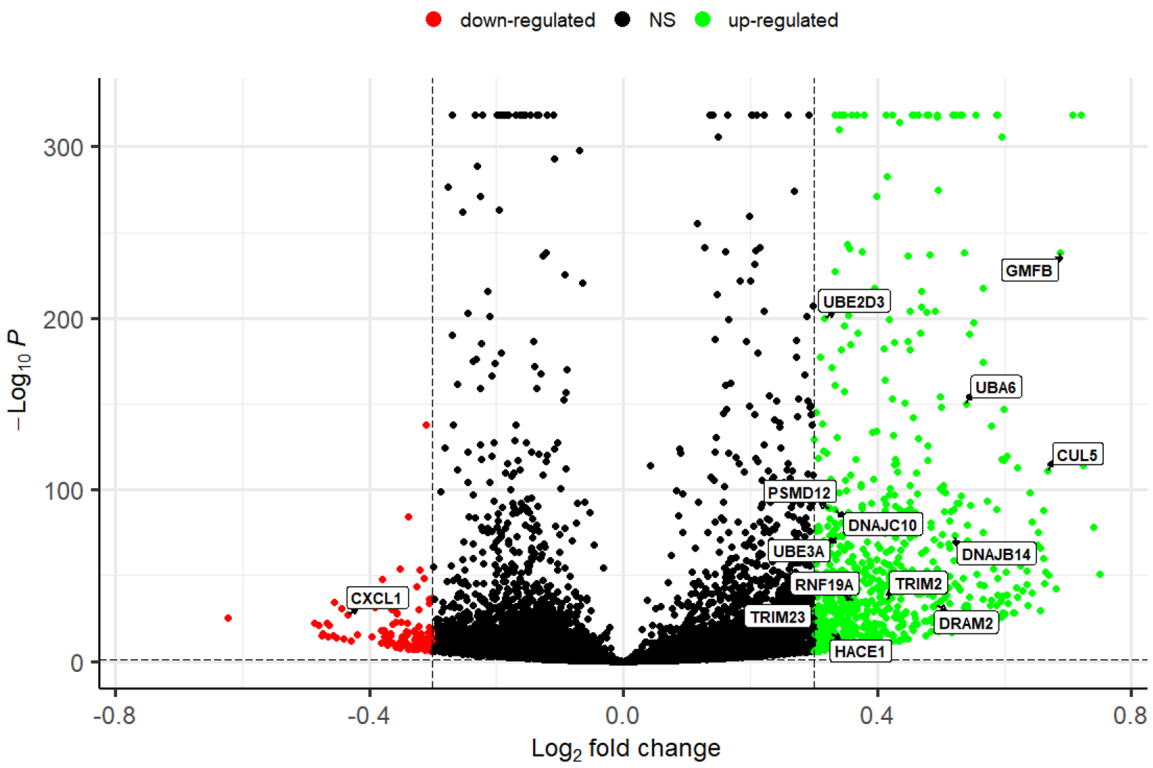

Supplementary Figure 3. TFP upregulates the expression of genes involved in autophagy/UPS pathways and down-regulates inflammatory response. After RNA extraction from fibroblasts cultured with or without TFP and cDNA library production, sequencing identified 546 differentially expressed genes (red: down-regulation; green: up-regulation; NS: not significant).

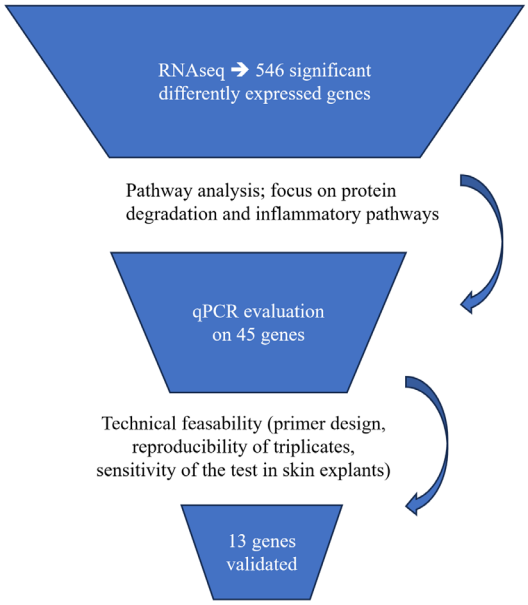

Supplementary Figure 4. Gene selection from the 546 genes identified in TFP-treated fibroblasts for further validation by qPCR in skin explants.

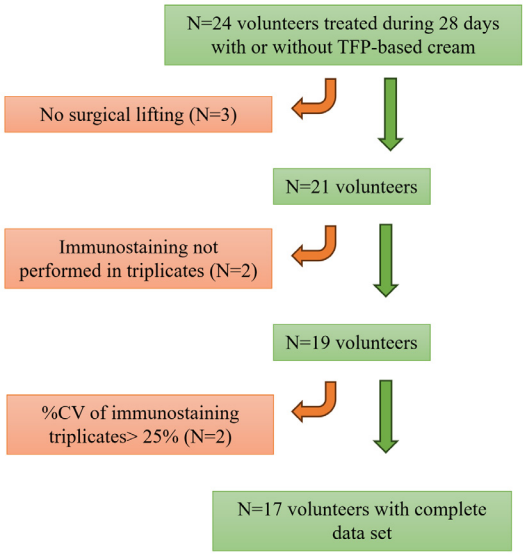

Supplementary Figure 5. Flow-chart of the cosmetic study.

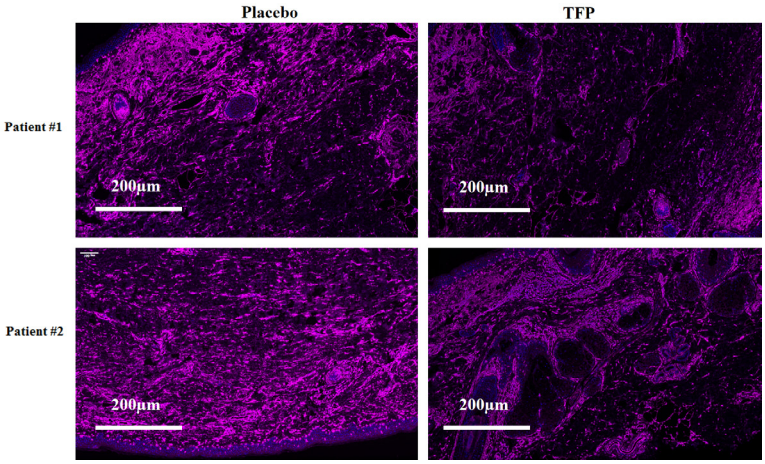

Supplementary Figure 6. TFP decreases vimentin in vivo. Skin explants from face lifting of the 17 volunteers were analyzed by immunolabelling using specific anti-vimentin antibody; Examples of vimentin detection (purple) in paired skin explants from 2 patients treated by TFP- and placebo-cream.

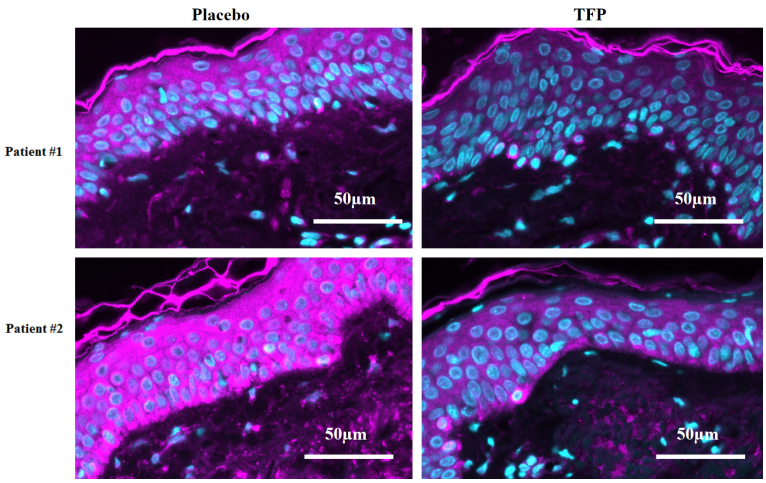

Supplementary Figure 7. TFP decreases glycation in vivo. Skin explants from face lifting of the 17 volunteers were analyzed by immunolabelling using specific anti-CML antibody; Examples of vimentin detection (purple) in paired skin explants from 2 patients treated by TFP- and placebo-cream.